Multiscale character of the nonlinear coherent dynamics in the Rayleigh-Taylor instability

S. I. Abarzhi,[1,2,*] K. Nishihara,[3] and R. Rosner[1]
[1]*FLASH, The University of Chicago, Chicago, Illinois, USA*
[2]*Center for Turbulence Research, Stanford University, Stanford, California, USA*
[3]*Institute for Laser Engineering, Osaka University, Osaka, Japan*
(Received 17 January 2005; published 22 March 2006)

We report nonlinear solutions for a system of conservation laws describing the dynamics of the large-scale coherent structure of bubbles and spikes in the Rayleigh-Taylor instability (RTI) for fluids with a finite density ratio. Three-dimensional flows are considered with general type of symmetry in the plane normal to the direction of gravity. The nonlocal properties of the interface evolution are accounted for on the basis of group theory. It is shown that isotropic coherent structures are stable. For anisotropic structures, secondary instabilities develop with the growth rate determined by the density ratio. For stable structures, the curvature and velocity of the nonlinear bubble have nontrivial dependencies on the density ratio, yet their mutual dependence on one another has an invariant form independent of the density ratio. The process of bubble merge is not considered. Based on the obtained results we argue that the large-scale coherent dynamics in RTI has a multiscale character and is governed by two length scales: the period of the coherent structure and the bubble (spike) position.

DOI: 10.1103/PhysRevE.73.036310 PACS number(s): 47.20.−k, 47.54.−r, 52.57.−z, 52.35.Py

I. INTRODUCTION

The Rayleigh-Taylor instability (RTI) and Richtmyer-Meshkov instability (RMI) develop whenever fluids of different densities are accelerated against the density gradient uniformly with time (RTI) or impulsively (RMI) [1,2]. Extensive interfacial mixing of the fluids ensues with time. The turbulent mixing plays a key role in many phenomena in physics and technology [3,4]. In inertial confinement fusion, it quenches ignition of deuterium-tritium fuel in laser-imploded targets. In astrophysics, it governs the explosion of supernovae and controls the formation of molecular clouds [3–5]. The turbulent mixing is the key feature of the impact dynamics of solids, mantle-lithosphere tectonics, premixed and nonpremixed combustion, oil production, and other applications [5]. A grip on the mixing process is the basic objective of studies of the Rayleigh-Taylor (RT) and Richtmyer-Meshkov (RM) instabilities [6]. The evolution of large-scale coherent structure, the dynamics of small-scale structures, and energy transfers are the fundamental issues to be understood [7,8].

The large-scale coherent structure is a characteristic of RT/RM flow. This is a periodic array of bubbles and spikes in the plane normal to the direction of acceleration: the heavy (light) fluid penetrates the light (heavy) fluid in bubbles (spikes). The structure is described by two, in general independent, length scales, its wavelength and the amplitude, which are the spatial period and the bubble (spike) position in the direction of acceleration, Fig. 1. The small-scale structures are produced by shear on the side of evolving spikes, and their rollup results in a mushroom-type shape of the spike. The energy is transferred to both large and small scales, and these transports are not well understood. Perhaps, the energy transfer to large scale can be associated with the influence of the initial conditions whereas that one to small scales is caused by shear.

The dynamics of RTI and RMI is governed by the system of conservation laws, which are nonlinear partial differential equations with initial and boundary conditions at the fluid interface. The nonlinearities, the baroclinic production of vorticity, and the secondary instabilities make the instability evolution essentially nonlocal and result in development of singularities in the governing equations. The nonlocality and singularities cause significant difficulties for theoretical and numerical studies of RTI and RMI. One of the key factors controlling the RT or RM dynamics is the ratio between the fluid densities [3,4,6]. To study the influence of the density ratio on the mixing process, several heuristic models were suggested [3,9]. These models interpreted the evolution of RTI and RMI as a single-scale problem, governed solely by the period of the coherent structure. Despite significant efforts and use of adjustable parameters, the models could not explain the observations completely [10]. In a recent attempt [11] to derive the postulates of the models [3,9] from the governing equations in a single-mode approximation, the complete set of the boundary conditions were not satisfied, and the conservation laws were thus violated.

Another approach to this long-standing problem was proposed by Ref. [8]. The analysis [8] applies the separation of scales in the governing equations and studies the large-scale coherent dynamics on the basis of group theory. In this sequel publication we consider in detail the approach and results of Ref. [8]. The present paper focuses on RTI. Our analysis accounts for the nonlocal properties of the flow and yields regular asymptotic solutions describing the dynamics of the bubble front in the general three-dimensional case. It is found that coherent structures in RTI are stable only if they are isotropic in the plane normal to the direction of gravity. Anisotropic structures are unstable. In the nonlinear regime,

*Fax: +1-773-834-3230. Email address: snezha@flash.uchicago.edu

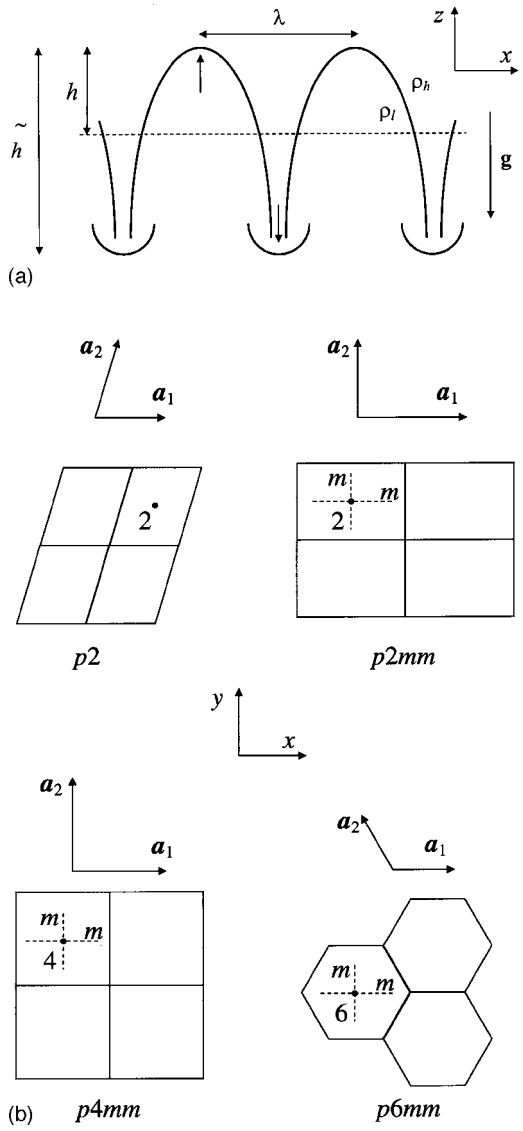

FIG. 1. The large-scale coherent structure of bubbles and spikes in the Rayleigh-Taylor instability. (a) A section of the interface in the plane (x,z) parallel to gravity $\mathbf{g}$: $\rho_{h(l)}$ is the density of the heavy (light) fluid, λ is the horizontal scale (wavelength or spatial period), $\tilde{h}$ is the vertical scale (amplitude), and h is the bubble position relative to the reference line (dashing line) which marks the initial position of the interface. Vertical arrows mark the direction of the fluid motion at the tip of the bubble (up) and spike (down). A rollup of vortices results in a mushroom-type shape of the spike. (b) Possible symmetry groups of the structure of bubbles and spikes in the plane (x,y) normal to gravity $\mathbf{g}$ and their basic elements: vectors of translations $\boldsymbol{a}_{1(2)}$, n-fold axis of rotation parallel to the z axis, $n=2$, 4, 6, mirror planes of reflection normal each other and parallel to the z axis (dashing lines). For groups $p4mm$ and $p6mm$ the values $|\boldsymbol{a}_{1(2)}|=\lambda$, whereas for groups $p2mm$ and $p2$ the values $|\boldsymbol{a}_{1(2)}|=\lambda_{x(y)}$.

for fluids with similar densities in the instabilities of anisotropic RT flows develop much slower than for fluids with highly contrasting densities. For stable RT structures, the curvature and velocity of the nonlinear bubble have nontrivial dependencies on the density ratio, yet the mutual dependence on one another has an invariant form independent of the density ratio. The results obtained indicate that the nonlinear coherent dynamics in RTI has a multiscale character. The bubble dynamics is governed by two independent length scales, the spatial period of the coherent structure and the bubble position. Our analysis explains existing data and identifies sensitive diagnostics for observations. The multibubbles interactions and the merger mechanism of the turbulent mixing are not considered.

II. NONLINEAR EVOLUTION OF RT UNSTABLE INTERFACE

According to observations [1,3,4,6,10,12–17], for incompressible fluids the Rayleigh-Taylor instability evolves as follows. In the linear regime, a small amplitude perturbation of the fluid interface grows exponentially with time t [1,3,4]. The instability growth rate is $\tau^{-1}\sim\sqrt{Ag/\lambda}$, where g is gravity, λ is the perturbation wavelength, and $A=(\rho_h-\rho_l)/(\rho_h+\rho_l)$ is the Atwood number with $\rho_{h(l)}$ being the density of the heavy (light) fluid [1]. The case of fluids with finite density ratio $0<A<1$ is most important for observations. The mode of the fastest growth set by surface tension and viscosity [4,18] defines the characteristic length scale $\lambda_{\max}$, and $\lambda\sim\lambda_{\max}$. In the nonlinear regime, a coherent structure of bubbles and spikes appears [1,6,12–17], Fig. 1. The bubbles move steadily, the spikes may accelerate, and the spatial period of the structure in the plane normal to the direction of gravity is λ [1,6,12–17], Fig. 1. Shear results in the Kelvin-Helmholtz instability, and vorticity is generated [13,15,17]. Small-scale structures appear on the side of evolving spikes, and the fluid energy is transported to scales smaller than λ [14–17], Fig. 1(a). For a broad band initial perturbation, the period λ of the coherent structure may increase, and the fluid energy may be transferred to larger scales [3,19]. Eventually, a mixing zone develops. In the chaotic regime, the width of the mixing zone in the direction of gravity grows quadratically with time [3,6,12], the period of the large-scale structure λ may not change any longer [6], and for fluids with similar densities, $A\approx 0$, the spectrum of small-scale structures is nearly Kolmogorov [17].

The secondary instabilities in the RT flow and hence the formations of singularities in the governing equations depend on the density ratio. For a system fluid-vacuum $A=1$ the spike singularities develop over an infinite time $t/\tau\to\infty$ [7,20–23] and influence the bubble dynamics and the spectral properties of the flow. In 1957 Garabedian [21] found that the singularities cause a nonuniqueness of asymptotic steady solutions describing the motion of a two-dimensional bubble. Layzer [20] used a simplified approach, the so-called single-mode approximation, disregarded the singularities, and obtained a unique steady solution. The long-standing discrepancy between the results of Refs. [20,21] was resolved by the analysis [7] based on group theory. It was shown that to capture the dynamics of the bubble front, the high-order correlations are essential to account for. The Layzer-type expansion [20] cannot be extended to higher orders: There is no a unique Layzer-type asymptotic solution, only a first-order approximation [7]. On the other side, the multiple harmonic asymptotic solutions [7] form a continuous family, similarly

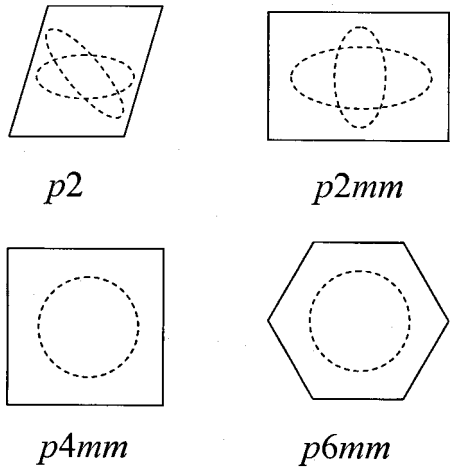

FIG. 2. Shape of the bubble front for various symmetry groups: dashing lines mark possible bubble contours in the plane (x,y). Dependent on the symmetry, near the tip the bubble shape is entirely described by a single principal curvature (groups $p6mm$ and $p4mm$ and $N_p=1$), by two principal curvatures (group $p2mm$, $N_p=2$), or by two principal curvatures and their position with respect to the axes (group $p2$, $N_p=3$).

to Garabedian's results [21]. The number of the family parameters is determined by symmetry of the two- or three-dimensional flow [7], Figs. 1(b) and 2. In a few special cases, the fastest stable solution in the family [7] and [21] is well approximated by the single-mode solution [20].

For fluids with similar densities, $A\approx 0$, the nature and evolution of singularities differ from those in the fluid-vacuum system, as discussed by Moore [24], Baker [25], and others [26–28] and references therein. For $A\approx 0$ the singularities are driven by shear and develop immediately for $t/\tau\sim 0^+$. They result in the occurrence of vortices [24,25] or Kelvin-Helmholtz spirals [27] and transfer energy to small scales [17]. For fluids with finite density ratio $0<A<1$ the quantitative character of the influence of singularities on the energy transports and large-scale coherent dynamics has yet to be elucidated [27–29]. Qualitatively, for $0<A<1$ the singularities develop at the fluid interface over a finite time $t/\tau\sim O(1)$ [27,28]. They govern the dynamics of small-scale structures with intense vorticity, influence the evolution of large-scale coherent structure, which is passively advected [29], and transport the fluid energy to both large and small scales [13–17]. Overall, the singularities make the interface evolution essentially nonlocal and sensitive to the processes occurred in the global flow. To obtain a reliable description of the large-scale coherent dynamics, we will account for the higher-order correlations and, based on symmetry arguments, will find the regular asymptotic solutions describing the nonlinear RT bubbles.

III. GOVERNING EQUATIONS AND LOCAL DYNAMICAL SYSTEM

In this section, we consider the governing equations and reduce the nonlinear partial differential equations to a system of ordinary differential equations describing the dynamics of the bubble (spike) locally, in a vicinity of its tip. Let (x,y,z) be the Cartesian coordinates and $\theta(x,y,z,t)=z^*(x,y,t)-z$ be a local scalar function with $\theta=0$ at the fluid interface $z^*(x,y,t)$. The fluid density and velocity have the form $\rho=\rho_h H(-\theta)+\rho_l H(\theta)$ and $\boldsymbol{\nu}=\boldsymbol{\nu}_h H(-\theta)+\boldsymbol{\nu}_l H(\theta)$, where H is the Heaviside step-function, and $\boldsymbol{\nu}_{h(l)}$ are the velocity of the heavy (light) fluid located in the region $\theta<0$ ($\theta>0$). For incompressible fluids, the values of $\rho_{h(l)}$ are independent of the coordinates and time and div $\boldsymbol{\nu}_{h(l)}=0$. The equation of continuity is reduced then to

$$\rho_h(\dot{\theta}+\boldsymbol{\nu}_h\cdot\nabla\theta)|_{\theta=0}=\rho_l(\dot{\theta}+\boldsymbol{\nu}_l\cdot\nabla\theta)|_{\theta=0}, \tag{1}$$

where the dot indicates a partial time-derivative [30]. The value of $\rho_{h(l)}(\dot{\theta}+\boldsymbol{\nu}_{h(l)}\cdot\nabla\theta)$ in Eq. (1) is the flux of mass of the heavy (light) fluid across the moving interface. If there is no mass flux across the interface, the normal component of velocity is continuous at the interface and

$$\boldsymbol{\nu}_h\cdot\nabla\theta|_{\theta=0}=\boldsymbol{\nu}_l\cdot\nabla\theta|_{\theta=0}=-\dot{\theta}|_{\theta=0}, \tag{2a}$$

If $\boldsymbol{n}$ is the unit normal of the interface with $\nabla\theta=\boldsymbol{n}|\nabla\theta|$, and $\tilde{\boldsymbol{\nu}}$ is the velocity of the interface with $\tilde{\boldsymbol{\nu}}\cdot\boldsymbol{n}=-\dot{\theta}/|\nabla\theta|$, then Eqs. (1), (2a) have respectively the form $\rho_l(\boldsymbol{\nu}_l\cdot\boldsymbol{n}-\tilde{\boldsymbol{\nu}}\cdot\boldsymbol{n})|_{\theta=0}=\rho_h(\boldsymbol{\nu}_h\cdot\boldsymbol{n}-\tilde{\boldsymbol{\nu}}\cdot\boldsymbol{n})|_{\theta=0}$ and $\boldsymbol{\nu}_l\cdot\boldsymbol{n}|_{\theta=0}=\boldsymbol{\nu}_h\cdot\boldsymbol{n}|_{\theta=0}=\tilde{\boldsymbol{\nu}}\cdot\boldsymbol{n}$ in agreement with Ref. [30].

Without mass flux across the interface and with the viscous stress and surface tension neglected, the momentum equation is transformed into the conditions

$$[\dot{\boldsymbol{\nu}}_h+(\boldsymbol{\nu}_h\cdot\nabla)\boldsymbol{\nu}_h+\boldsymbol{g}]\rho_h+\nabla p_h|_{\theta<0}, \tag{2b}$$

$$[\dot{\boldsymbol{\nu}}_l+(\boldsymbol{\nu}_l\cdot\nabla)\boldsymbol{\nu}_l+\boldsymbol{g}]\rho_l+\nabla p_l|_{\theta>0}=0,\quad p_h|_{\theta=0}=p_l|_{\theta=0},$$

where $p_{h(l)}$ is the pressure of the heavy (light) fluid, and $\boldsymbol{g}$ is the gravity directed from the heavy fluid to the light one with $|\boldsymbol{g}|=g$ [30]. The boundary conditions at the infinity close the set of governing equations

$$\boldsymbol{\nu}|_{\theta\to-\infty}=\boldsymbol{\nu}_h|_{z\to+\infty}=0,\quad \boldsymbol{\nu}|_{\theta\to+\infty}=\boldsymbol{\nu}_l|_{z\to-\infty}=0. \tag{2c}$$

According to Eq. (2c), the flow has no mass sources [30].

The initial conditions define the spatial period, the time scale, and the symmetry of the fluid motion, Fig. 1. We choose the value of the spatial period as $\lambda\sim\lambda_{\max}$ [18], so the time scale in Eqs. (1), (2) is $\tau\sim\sqrt{\lambda/Ag}$ [1]. Based on the observations [12–17], we separate scales and divide the fluid interface into the active and passive regions [29]. The dynamics of active regions (small scales) is driven by vorticity while the passive regions (large scales) are simply advected. The velocity can be represented in the form $\boldsymbol{\nu}_{h(l)}=\nabla\Phi_{h(l)}+\nabla\times\boldsymbol{\Psi}_{h(l)}$, where the vector field $\boldsymbol{\Psi}_{h(l)}$ describes the dynamics at small scales $\ll\lambda$, and the scalar field $\Phi_{h(l)}$ describes the coherent motion at large scales $\sim\lambda$. In order to be stable under modulations with length scales much larger than λ the coherent motion in Eqs. (1), (2) must be invariant under one of spatial symmorphic groups with translations in the plane (x,y) and inversion $r\to-r$, $r=(x,y)$ and $y\to-y$ [7,8,31]. The symmorphic groups have no glide planes and screw axes [31]. For a three-dimensional (3D) flow these are hexagonal $p6mm$, square $p4mm$, rectangular $p2mm$, and a

few other groups, see Fig. 1(b). For a 2D flow this is the group $pm11$ [31,32].

In a vicinity of the tip of the bubble (spike) the fluid motion is nearly potential, the contribution of small-scale components is insignificant, and the large-scale coherent dynamics is identical to the all-scale dynamics of the entire interface. To find the nonlinear solutions describing the asymptotic evolution of the bubble front in RTI, we reduce the nonlinear partial differential equations in Eqs. (1), (2) to a local dynamical system, similarly to Refs. [7,8]. All calculations are performed in the frame of reference moving with velocity $\nu(t)$ in the z direction, where $\nu(t)$ is the velocity at the bubble tip in the laboratory frame of references, and $\nu(t)=dh(t)/dt$ with $h(t)$ being the bubble position. In the case of a 3D flow with square symmetry $p4mm$

$$\Phi_h=\sum_{m=0}^{\infty}\sum_{n=0}^{\infty}\Phi_{mn}(t)[z+\exp(-\alpha_{mn}kz)\cos(mkx)\times\cos(nky)/k\alpha_{mn}]+f_h(t),$$

$$\Phi_l=\sum_{m=0}^{\infty}\sum_{n=0}^{\infty}\tilde{\Phi}_{mn}(t)[-z+\exp(\alpha_{mn}kz)\cos(mkx)\times\cos(nky)/k\alpha_{mn}]+f_l(t), \quad (3)$$

where $\alpha_{mn}=\sqrt{m^2+n^2}$, m and n are integers, $k=2\pi/\lambda$ is the wave vector, the Fourier amplitudes $\Phi_{mn}=\Phi_{nm}$ and $\tilde{\Phi}_{mn}=\tilde{\Phi}_{nm}$ due to symmetry with $\Phi_{00}=\tilde{\Phi}_{00}=0$, and $f_{h(l)}$ are time-dependent functions. The bubble tip is a point of stagnation with coordinates $(0,0,0)$ in the unit cell. For $x,y\sim 0$, the interface can be expanded as a power series, $z^*=\Sigma_{N=1}^{\infty}\Sigma_{i+j=N}\zeta_{ij}(t)x^{2i}y^{2j}$, where $\zeta_{ij}=\zeta_{ji}$ due to symmetry, $\zeta_{10}=\zeta_1$ is the principal curvature at the bubble tip, and $N=i+j$ is the order of approximation with $1\leqslant N<\infty$. Using the foregoing expressions, we take the first integral of Eqs. (2b), expand Eqs. (1), (2) for $x,y\sim 0$, and derive a system of ordinary differential equations for the variables $\zeta_{ij}(t)$ and moments $M_{a,b,c}(t)=\Sigma_{m=0}^{\infty}\Sigma_{n=0}^{\infty}\Phi_{mn}k^{a+b+c}m^a n^b\alpha_{mn}^c$ and $\tilde{M}_{a,b,c}(t)=\Sigma_{m=0}^{\infty}\Sigma_{n=0}^{\infty}\tilde{\Phi}_{mn}k^{a+b+c}m^a n^b\alpha_{mn}^c$, where a, b, and c are integers. The moments are the correlation functions. Due to symmetry $M_{a,b,c}=M_{b,a,c}$ and $M_{a+2,b,c}+M_{a,b+2,c}=M_{a,b,c+2}$ and similarly for $\tilde{M}_{a,b,c}$. For $N=1$, the mass conservation (1) takes the form

$$(\dot{\zeta}_1-4\zeta_1M_1-M_2/2)\rho_h=(\dot{\zeta}_1-4\zeta_1\tilde{M}_1+\tilde{M}_2/2)\rho_l, \quad (4)$$

and the conditions in Eqs. (2) with no mass flux across the interface and with no mass source are, respectively,

$$\dot{\zeta}_1=4\zeta_1M_1+M_2/2=4\zeta_1\tilde{M}_1-\tilde{M}_2/2, \quad (5a)$$

$$(-\dot{M}_1/2-\zeta_1\dot{M}_0+M_1^2/2+\zeta_1 g)\rho_h=(-\dot{\tilde{M}}_1/2+\zeta_1\dot{\tilde{M}}_0+\tilde{M}_1^2/2+\zeta_1 g)\rho_l, \quad (5b)$$

$$M_0=-\tilde{M}_0=-\nu=-\dot{h}, \quad (5c)$$

where the notations $M_0=M_{0,0,0}$, $M_1=M_{2,0,-1}$, $M_2=M_{2,0,0}$ and analogously for $\tilde{M}$'s. The presentation in terms of moments M's and $\tilde{M}$'s and surface variables ζ's allows one to study the interplay of harmonics, to account for the nonlocal character of the nonlinear dynamics, and to derive regular asymptotic solutions with a desired accuracy. In every order of approximation, $N\geqslant 1$, the number of moments in the dynamical system is larger than the number of equations. To find the nonlinear asymptotic solution for $(t/\tau)\to\infty$ one should solve the closure problem and establish the proper relations between the moments.

IV. LAYZER-TYPE SINGLE-MODE SOLUTIONS FOR $A<1$

In this section, we show that for $A<1$ the Layzer-type single-mode solution can be found only if one of the boundary conditions (2) is violated. Readers interested in multiple harmonic solutions, which obey the conservation laws (2), may skip this section.

For a fluid-vacuum system the limitations of Layzer's approach [20] are well known, see Sec. II and Refs. [7,21–23] for detail. Still, the solution obtained by Layzer for $A=1$ [20] was used by empirical models [3,9,10] to adjust the values of free parameters in the heuristic equation, balanced for $A<1$ the flow inertia, buoyancy, and drag. The assumptions of the models are worth to check, and we reduce our dynamical system to the expansion of the Layzer type. The Layzer-type expansion [20] cannot be extended to our dynamical system (5).

In Layzer-type approximation, we truncate the velocity potentials and retain in the expressions for the moments only the first-order amplitudes, that is $N=1$ and $m+n=1$ in Eqs. (4), (5). With $M_0=2\Phi_{10}$, $M_1=\Phi_{10}k$, $M_2=\Phi_{10}k^2$, and similarly for $\tilde{M}$, one finds from Eq. (4)

$$8A\dot{\zeta}_1-(1+A)[8(\zeta_1/k)+1]k^2M_0+(1-A)[8(\zeta_1/k)-1]k^2\tilde{M}_0=0, \quad (6)$$

and from Eqs. (5), respectively,

$$\dot{\zeta}_1=2kM_0(\zeta_1+k/8)=2k\tilde{M}_0(\zeta_1-k/8), \quad (7a)$$

$$(1+A)[-\dot{M}_0k(\zeta_1/k+1/4)+k^2M_0^2/8]-(1-A)\times[\dot{\tilde{M}}_0k(\zeta_1/k-1/4)+k^2\tilde{M}_1^2/8]+2Ag\zeta_1=0, \quad (7b)$$

$$M_0=-\tilde{M}_0=-\nu. \quad (7c)$$

In the Layzer-type expansion, one can integrate Eqs. (6), (7b), (7c) and derive thus a solution which conserves mass, Eqs. (1), (4), momentum Eqs. (7b), and has no mass sources, Eqs. (5c) (see Ref. [33] for more detail). For $t\gg\tau$, the system Eqs. (6), (7b), (7c) has two asymptotic solutions: a regular solution for a bubble and a singular solution for a spike. The curvature and velocity of the Layzer-type bubble are

$$\zeta_1 = \zeta_L = -Ak/8, \quad \nu = \nu_L = \sqrt{Ag/k}. \tag{8a}$$

The velocity ν_L in Eq. (8a) has the re-scaling $g \to Ag$, and agrees therefore with the empirical model [3]. The curvature and velocity of the Layzer-type spike are

$$\zeta_1 \sim k \exp(2gkt^2/A), \quad \nu \sim gt, \tag{8b}$$

and the spike velocity in Eq. (8b) is independent of the density ratio. However, the single-mode solutions Eqs. (8) violate the condition of continuity of the normal component of velocity Eqs. (2a), (5a), (7a) and require a flux of mass across the interface. Substituting the expressions Eqs. (8) in Eqs. (2a), (3), one finds that for regular bubble the mass flux is steady $\sim\rho\sqrt{Ag/k}(1-A^2)(x^2+y^2)k^2$, while for singular spike it grows with time $\sim\rho gt(1-A^2)e^{2gkt^2/A}(x^2+y^2)k^2$, where $\rho=(\rho_h+\rho_l)/2$.

It is obvious from Eqs. (7a), (7c) that in the Layzer-type approximation the two boundary conditions (the continuity of the normal component of velocity at the interface and no mass sources in the flow) cannot be satisfied at the same time in the nonlinear regime. Another "Layzer-type" model in Ref. [11] met with the same difficulty. To avoid this issue, the model [11] added an artificial term in the potential of the light fluid and introduced a nonuniform time-dependent mass flow at the infinity. In this way, the boundary condition in Eq. (2c) and, respectively, in Eqs. (5c) and (7c) was violated, and the solution [11] agreed with the assumptions of the drag model [9]. In Refs. [9,11], the curvature of the RT bubble is $\zeta_1=\zeta_D=\zeta_L|_{A=1}$ and its velocity is $\nu=\nu_D=\sqrt{2A/(1+A)}\sqrt{g/k}$.

We conclude that in a two-fluid system $A<1$ the Layzer-type single-mode solutions do not satisfy simultaneously the conditions of continuity of the normal component of velocity at the fluid interface and no time-dependent mass sources in the flow and do not obey therefore the conservation laws (2).

V. MULTIPLE HARMONIC SOLUTIONS

To find regular asymptotic solutions describing the nonlinear evolution of the bubble front, one should account for the high-order correlations and the nonlocal properties of the flow that has singularities [8]. The singularities influence the interplay of harmonics in the global flow as well as in the local dynamical system (5), and determine therefore the velocity and shape of the regular bubble. We assume that the bubble shape is free and find a continuous family of regular asymptotic solutions for system (5). This family contains all local solutions allowed by symmetry of the global flow. The family is parametrized by the principal curvatures in the principal normal sections of the interface, and by the position of these normal sections with respect to the Cartesian (crystallographic) axes [7,8], Fig. 2. The parameters describe entirely the shape of the bubble front in a vicinity of its tip. The number of the parameters N_p is $N_p \leqslant 3$ in the general case, similarly to Refs. [7,21] for $A=1$, Fig. 2. We perform the stability analysis and choose the fastest stable solution in the family as being the physically significant one [8].

To build the family of regular asymptotic solutions, we truncate the expressions for the moments in Eqs. (5) so that in every order of approximation N the number of equations N_e and the number of variables N_t (i.e., the Fourier amplitudes $\Phi_{mn}, \tilde{\Phi}_{mn}$ and surface variables ζ_{ij}) obey the relation $N_t=N_e+N_p$, where N_p is the number of the family parameters, Figs. 1 and 2. For solutions in the family the interplay of harmonics is well captured, and the lowest-order harmonics are dominant and insensitive to a particular choice of higher-order amplitudes used in the truncation.

A. Regular asymptotic solutions for isotropic 3D flows with square symmetry

For a 3D flow with square symmetry $N_p=1$, see Fig. 2. To find the regular asymptotic solutions for system (5), we impose conditions $\dot{\zeta}_{ij}=\dot{M}_{a,b,c}=\dot{\tilde{M}}_{a,b,c}=0$, keep the relation $\zeta_1=-M_2/8M_1=\tilde{M}_2/8\tilde{M}_1$ as a free parameter, and thus obtain the velocity ν, the amplitudes Φ_{mn}, $\tilde{\Phi}_{mn}$, and the surface variables ζ_{ij} as functions of this parameter. For $N=1$ the number of equations in system (5) is $N_e=4$, so the truncation number is $N_t=N_e+N_p=5$ and $m+n=2$. With $M_0=\Phi_{10}+\Phi_{20}=(3M_1/k)(1-M_2/3M_1k)$ and $\tilde{M}_0=\tilde{\Phi}_{10}+\tilde{\Phi}_{20}=(3\tilde{M}_1/k)(1-\tilde{M}_2/3\tilde{M}_1k)$, one finds from Eqs. (5) the bubble velocity and the amplitudes as functions of the bubble curvature and Atwood number:

$$\nu = \sqrt{\frac{g}{k}}\left(\frac{-2A(\zeta_1/k)}{A[3-8(\zeta_1/k)]^2-48(1-A)(\zeta_1/k)}\right)^{1/2} \times[9-64(\zeta_1/k)^2], \tag{9}$$

$$\Phi_{10} = 2\sqrt{\frac{g}{k}}\left(\frac{-2A(\zeta_1/k)}{A[3-8(\zeta_1/k)]^2-48(1-A)(\zeta_1/k)}\right)^{1/2} \times[1+4(\zeta_1/k)][3-8(\zeta_1/k)], \quad \Phi_{20} = -\nu-\Phi_{10},$$

$$\tilde{\Phi}_{10} = -2\sqrt{\frac{g}{k}}\left(\frac{-2A(\zeta_1/k)}{A[3-8(\zeta_1/k)]^2-48(1-A)(\zeta_1/k)}\right)^{1/2} \times[1-4(\zeta_1/k)][3+8(\zeta_1/k)], \quad \tilde{\Phi}_{20} = \nu-\tilde{\Phi}_{10}.$$

For $N>1$, the family of solutions can be found analogously. For any value of the Atwood number A in the interval $\zeta_{cr}<\zeta_1\leqslant 0$ the absolute values of the Fourier amplitudes $\Phi_{mn}, \tilde{\Phi}_{mn}$ decay exponentially with increase in their order $m+n$, and the lowest-order amplitudes Φ_{10} and $\tilde{\Phi}_{10}$ are dominant. Similarly to Ref. [7], solutions with very small and with finite curvature values are well approximated for $N>1$. For $\zeta_1 \sim \zeta_{cr}$ the convergence is broken, where $\zeta_{cr}=\zeta_{cr}(A)$ with $\zeta_{cr}=-k/6$ for $A\approx 1$ and $\zeta_{cr}\approx 0$ for $A\approx 0$. For fluids with highly contrasting densities $A\approx 1$, the values of the Fourier amplitudes of the light fluid are much larger than those of the heavy fluid, so that $|\Phi_{mn}| \sim |\tilde{\Phi}_{(m+1)n}|$. For fluids with similar densities $A\approx 0$, this difference is insignificant, and $|\Phi_{mn}| \sim |\tilde{\Phi}_{mn}|$.

For fastest solution in Eqs. (9) $(\partial\nu/\partial\zeta_1)=0$ and $(\partial^2\nu/\partial\zeta_1^2)<0$. This solution is given by

$$\zeta_1 = \zeta_A, \quad \nu = \upsilon_{\zeta_1=\zeta_A} = \nu_A. \tag{10}$$

The value $\zeta_A=Ck$ where C is the real negative root of the equation

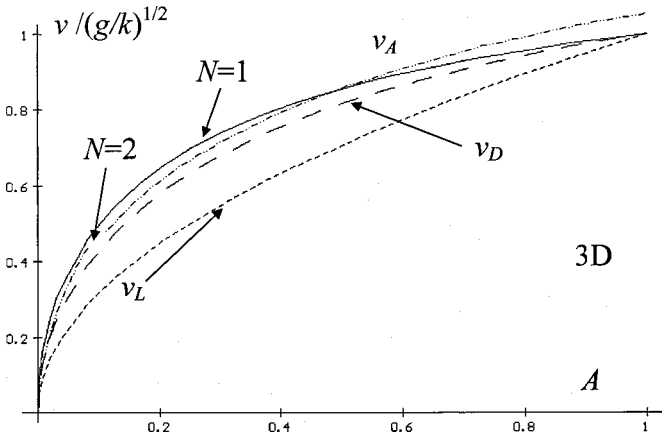

FIG. 3. Dependence of bubble velocity v on the Atwood number A for isotropic highly symmetric 3D flows; k is the wave vector, g is gravity, N is the order of approximation; v_A is the multiple harmonic nonlocal solution, the solid line marks $N=1$, Eqs. (10), the dash-dot-dotted line marks $N=2$; $v_L=\sqrt{Ag/k}$ is the Layzer-type solution, Eq. (8a), [3]; $v_D=\sqrt{2Ag/(1+A)k}$ is given by drag models [9,11].

$$C^4 - C^3/A + (9/32)C^2 - (3/16)^3 = 0. \tag{11}$$

The explicit analytical expressions for ζ_A and v_A are cumbersome and the subscript A in Eq. (10) emphasizes complex dependencies of the bubble curvature and velocity on the Atwood number, Figs. 3 and 4. For all values of the Atwood number A, the velocity v_A has a universal dependence on the curvature ζ_A:

$$v_A = \sqrt{g/k}(8|\zeta_A|/k)^{3/2}. \tag{12}$$

In the limiting case of fluids with highly contrasting densities $A \approx 1$, the solution (10) takes the form

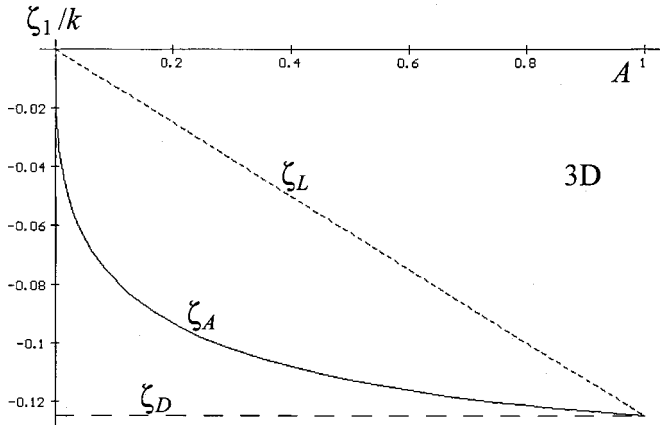

FIG. 4. Dependence of the bubble curvature on the Atwood number A for isotropic highly symmetric 3D flows; k is the wave vector; $\zeta_L=-Ak/8$ is the Layzer-type solution, Eq. (8a); $\zeta_D=-k/8$ is given by drag models [9,11]; ζ_A is the multiple harmonic nonlocal solution, Eq. (10).

$$\zeta_A \approx -(k/8)[1-(1-A)/8], \quad v_A \approx \sqrt{g/k}[1-3(1-A)/16]. \tag{13a}$$

In the other limiting case $A \approx 0$, it can be expanded as

$$\zeta_A \approx -(3k/16)A^{1/3}, \quad v_A \approx (3/2)^{3/2}\sqrt{Ag/k}. \tag{13b}$$

Higher-order corrections for the velocity of solutions (12) are small. With third-order harmonics involved and with up to fourth-order moments, the value of v_A increases on $\sim 5\%$ for $A \sim 1$, in agreement with Ref. [7], and decreases on $\sim 15\%$ for $A \sim 0$ and becomes $\sim 1.57\sqrt{Ag/k}$, see Fig. 4.

To analyze the stability of the solutions thus obtained, we perturb ζ_{ij}, $M_{a,b,c}$, and $\tilde{M}_{a,b,c}$ slightly, so that $\zeta_{ij} \to \zeta_{ij} + \theta_{ij}(t)$, $M_{a,b,c} \to M_{a,b,c} + \Delta_{a,b,c}(t)$, $\tilde{M}_{a,b,c} \to \tilde{M}_{a,b,c} + \tilde{\Delta}_{a,b,c}(t)$. For every N, we leave the smallest in magnitude higher-order amplitude unperturbed, and establish additional relations between $\Delta_{a,b,c}$ and $\tilde{\Delta}_{a,b,c}$, so the number of independent Δ's, $\tilde{\Delta}$'s and θ's equals N_e. We derive then from Eqs. (2) θ_{ij}, $\Delta_{a,b,c}$, $\tilde{\Delta}_{a,b,c} \sim \exp[\omega(t/\tau)]$, where the Liapunov exponents are $\omega = \omega(\sqrt{gk}, A, (\zeta_1/k))$. For stable solutions $\mathrm{Re}[\omega] < 0$.

For $N=1$, the smallest amplitude in the steady family (9) is Φ_{20}, $|\Phi_{20}| \ll |\Phi_{10}|$, $|\tilde{\Phi}_{10(20)}|$, and slightly perturbing $\zeta_1 \to \zeta_1 + \theta_1(t)$, $\tilde{\Phi}_{10} \to \tilde{\Phi}_{10} + \tilde{\varphi}_{10}(t)$, $\tilde{\Phi}_{20} \to \tilde{\Phi}_{20} + \tilde{\varphi}_{20}(t)$, and $\Phi_{10} \to \Phi_{10} + \varphi_{10}(t)$, we find from Eqs. (5), (9) that the Liapunov exponents obey the quadratic equation $\omega^2 a_2 + \omega a_1 + a_0 = 0$, with coefficients a_2, a_1, a_0 dependent on the Atwood number A and curvature ζ_1/k. Solutions with $\zeta_1 \sim \zeta_{cr}$ and $\zeta_1 \sim 0$ appear unstable, and solutions with $\zeta_1 \sim \zeta_A$ are stable. For $N > 1$, the stability analysis can be performed analogously. With increase in N the interval of stability is narrowing, whereas solutions with $\zeta_1 \sim \zeta_A$ remain stable.

Therefore in the family (9) the solution (10) is the physically significant one. The invariant (12) given by this solution $v_A^2/g\lambda^4|\zeta_A|^3 = (dh/dt)^2/g\lambda^4|\zeta_A|^3 = 1/2\pi^4$ indicates that the nonlinear RT dynamics is a multiscale process governed by two independent length scales: the horizontal scale λ and vertical scale h. It shows as well that the shape of the bubble front depends on the Froude number $\mathrm{Fr} = (dh/dt)^2/g\lambda$ as $|\zeta_A| \sim \mathrm{Fr}^{1/3}/\lambda$.

B. Regular asymptotic solutions for isotropic 3D flows with high symmetries

The foregoing analysis can be applied for 3D flows with other symmetries and 2D flows. For isotropic 3D flows with high symmetries (square $p4mm$ and hexagonal $p6mm$ groups) the asymptotic dynamics (i.e., the nonlinear solutions and their stability) coincide quantitatively except for the difference in the normalization factor k. As discussed in Refs. [7,8], the reason of this universality is a nearly isotropic shape of the bubble front in the plane normal to the direction of gravity. For hexagonal symmetry $k = 4\pi/\lambda\sqrt{3}$, for square symmetry $k = 2\pi/\lambda$, and for tubular flow $k = 2\beta_0/\lambda$, where β_0 is the first zero of the Bessel function J_0, Figs. 1 and 2.

C. Regular asymptotic solutions for 2D flow

The derivation of regular asymptotic solutions in two dimensions is similar to that in three dimensions [7,8,34]. For

a 2D flow with symmetry $pm11$, the fluid potentials are $\Phi_h=\Sigma_{m=1}^{\infty}\Phi_m(t)[z+\exp(-mkz)\cos(mkx)/km]+f_h(t)$ and $\Phi_l=\Sigma_{m=1}^{\infty}\tilde{\Phi}_m(t)[-z+\exp(mkz)\cos(mkx)/km]+f_l(t)$. The fluid interface has the form $z^*=\Sigma_{N=1}^{\infty}\zeta_N(t)x^{2N}$ near the bubble tip. For $N=1$ for solutions in the one-parameter 2D family, the values of velocity and Fourier amplitudes have the form

$$\nu=\frac{3}{2}\sqrt{\frac{g}{k}}\left(\frac{-2A(\zeta_1/k)}{A[1-2(\zeta_1/k)]^2-4(1-A)(\zeta_1/k)}\right)^{1/2}\times[1-4(\zeta_1/k)^2], \tag{14}$$

$$\Phi_1=2\sqrt{\frac{g}{k}}\left(\frac{-2A(\zeta_1/k)}{A[1-2(\zeta_1/k)]^2-4(1-A)(\zeta_1/k)}\right)^{1/2}\times[1+(\zeta_1/k)-6(\zeta_1/k)^2],\quad \Phi_2=-\nu-\Phi_1,$$

$$\tilde{\Phi}_1=2\sqrt{\frac{g}{k}}\left(\frac{-2A(\zeta_1/k)}{A[1-2(\zeta_1/k)]^2-4(1-A)(\zeta_1/k)}\right)^{1/2}\times[-1+(\zeta_1/k)+6(\zeta_1/k)^2],\quad \tilde{\Phi}_2=\nu-\tilde{\Phi}_1.$$

The stability analysis for the 2D family (14) is similar to that for the 3D family (9). The fastest stable, solution in the family (14) is the solution with

$$\zeta_1=\zeta_A,\quad \nu=v|_{\zeta_1=\zeta_A}=\nu_A, \tag{15}$$

where $\zeta_A=Ck$ and C obeys the equation

$$C^4-(4/3)C^3/A+(1/2)C^2-(1/48)=0. \tag{16}$$

The mutual dependence of the curvature and velocity in Eqs. (15), (16) has the form

$$\nu_A=3\sqrt{g/k}(2|\zeta_A|/k)^{3/2}. \tag{17}$$

In higher approximations the value of ν_A increases on $\sim 6\%$ for $A\sim 1$, in agreement with Refs. [7,21], and decreases on $\sim 16\%$ for $A\sim 0$.

Comparing the 2D results in Eqs. (14)–(17) with the 3D results in Eqs. (9)–(13), we obtain in main order

$$[\zeta_A]_{3D}/[\zeta_A]_{2D}\approx 3/4,\quad [\nu_A]_{3D}/[\nu_A]_{2D}\approx\sqrt{3}, \tag{18}$$

similarly to Ref. [7] for $A=1$. Figure 5 and Table I present the Fourier amplitudes $\Phi_{n,A}$, $\tilde{\Phi}_{n,A}$ with $n=1$, 2, 3 and $N=2$ for the 2D and isotropic highly symmetric 3D flows. For a transparent comparison between the 2D and 3D cases, we choose hexagonal symmetry $p6mm$, for which the contribution of "nondiagonal" amplitudes is insignificant [8]. Figure 5 and Table I show that properties of the 2D and 3D solutions are very similar. For instance, the ratios $|\Phi_{n,A}/\Phi_{1,A}|$ and $|\tilde{\Phi}_{n,A}/\tilde{\Phi}_{1,A}|$ are the same in 2D and 3D cases. It is known, however, that 2D flows in RTI are unstable under 3D modulations. To study the properties of the dimensional 2D-3D crossover in RTI, we consider the nonlinear dynamics of anisotropic 3D flows.

D. Regular asymptotic solutions for anisotropic 3D flows with low symmetries

For several anisotropic 3D flows with low symmetries, the coherent structures might be stable under modulations with very large length scales. These are symmetry groups of rectangle $p2mm$, rhomb cmm, and parallelogram $p2$, which have inversion in the plane normal to the direction of gravity $(r\rightarrow -r, r=(x,y)$ [7,8,31,32], see Figs. 1(b) and 2. In this section, we show that in RTI only isotropic coherent structures are stable. For anisotropic 3D structures, secondary instabilities develop, and their growth rate depends on the density ratio, the aspect ratio, and the bubble shape.

For a 3D flow with rectangular symmetry $p2mm$, the continuous family of regular asymptotic solutions is described by the two parameters, the principal curvatures $\zeta_{1x(y)}$ in the $x(y)$ directions and $N_p=2$ [7,8,32], Figs. 1(b) and 2. The velocity and the Fourier amplitudes of the solutions in the two-parameter family have cumbersome dependencies on the principal curvatures $\zeta_{1x(y)}$, wave vectors $k_{x(y)}$, and the Atwood number A and are not presented here. The bubble shape is described by the aspect ratio k_y/k_x and by the ratio between the curvatures ζ_{1y}/ζ_{1x}. For $0<k_y/k_x<1$, the bubbles with $(\zeta_{1y}/\zeta_{1x})(k_x/k_y)^2=1$ have a circular contour, while the contour of bubbles with $(\zeta_{1y}/\zeta_{1x})(k_x/k_y)^2<1$ (>1) is elongated in the y (x) direction. As $\zeta_{1y}k_x/k_y^2\rightarrow 0$, the interface flattens in the y direction and the bubble becomes two dimensional, Fig. 2, [7,32].

For general values of $(\zeta_{1y}/\zeta_{1x})(k_x/k_y)^2$ and k_y/k_x, the anisotropic solutions are unstable. For nearly isotropic flows with $k_x\sim k_y\sim k$ and $\zeta_{1x}\sim\zeta_{1y}\sim\zeta_1$, the expansion of velocity in terms of small (k_x-k_y) and $(\zeta_{1x}-\zeta_{1y})$ starts from terms of second order,

$$\nu-\nu_{3Ds}\sim F_\zeta(\zeta_{1x}-\zeta_{1y})^2+F_k(k_x-k_y)^2, \tag{19}$$

where ν_{3Ds} is the velocity given by the 3D square family (9) with $k=(k_x+k_y)/2$ and $\zeta_1=(\zeta_{1x}+\zeta_{1y})/2$, and $F_{\zeta(k)}=F_{\zeta(k)}(A,g,k,\zeta_1)$ with $F_{\zeta(k)}<0$. In this nearly isotropic case, only solutions with $\zeta_1\sim\zeta_A$ and $\nu\approx\nu_A$ from Eq. (10) are stable.

In the other limiting case of nearly two-dimensional bubbles with $\zeta_{1y}k_x/k_y^2\rightarrow 0$, the velocity can be expanded as

$$\nu-\nu_{2D}\sim F_{2D}\zeta_{1y}k_x/k_y^2, \tag{20}$$

where ν_{2D} is velocity for the 2D family in Eqs. (14) with $\zeta_1=\zeta_{1x}$ and $k=k_x$, and $F_{2D}=F_{2D}(A,g,k,\zeta_1)$ with $F_{2D}>0$. The Liapunov exponent associated with the dimensional 2D-3D crossover has the form

$$\omega_{3D\text{-}2D}=(k_y/k_x)\sqrt{Agk_x}[f_x-(\zeta_{1y}k_x^2/\zeta_{1x}k_y^2)f_y], \tag{21}$$

where $f_{x(y)}=f_{x(y)}(A,\zeta_1/k)$, $f_{x(y)}>0$, and $f_x>f_y$ for $\zeta_{cr}<\zeta_1\leqslant 0$. For 2D bubbles flat in the y direction with $\zeta_{1y}\equiv 0$ and curved in the x direction with $\zeta_{1x}=\zeta_1=\zeta_A$ from Eq. (15), the increment of the 2D-3D instability in Eq. (21) has a complicated dependence on the Atwood number, Fig. 6:

$$\omega_{3D\text{-}2D}=(k_y/k_x)f_A(A)\sqrt{Agk_x}. \tag{22}$$

For $0.3<A\leqslant 1$ the value of $\omega_{3D\text{-}2D}$ is nearly constant. In the limiting case of fluids with highly contrasting densities $A\sim 1$,

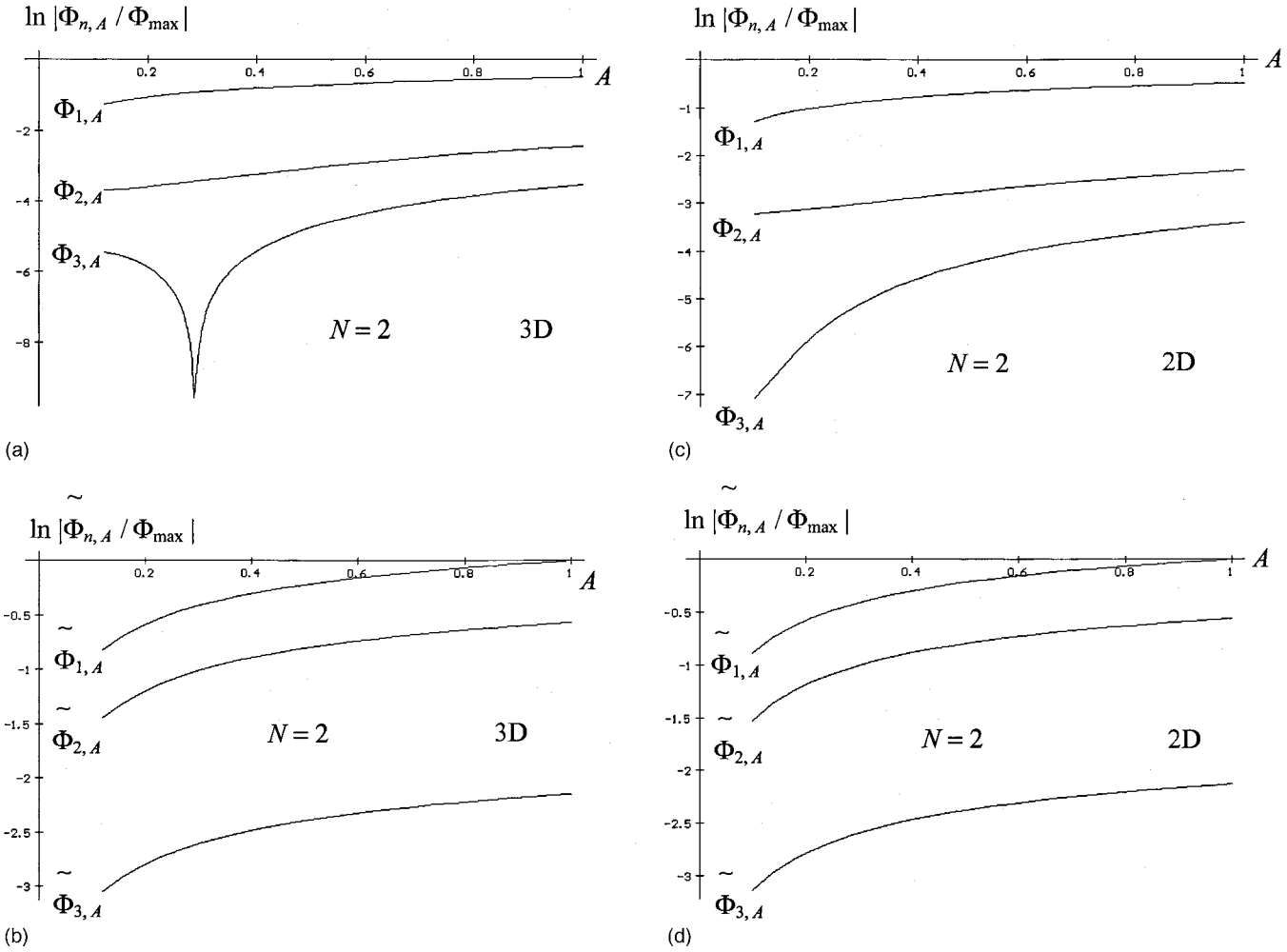

FIG. 5. Exponential decay of Fourier amplitudes $\Phi_{n,A}$ and $\tilde{\Phi}_{n,A}$ with increase in n for physically significant solutions in the multiple harmonic family: (a), (b) isotropic highly symmetric 3D flow p6mm; $\Phi_{\max}=\tilde{\Phi}_1|_{A=1}\approx 1.92\sqrt{g/k}$; (c), (d) 2D flow; $\Phi_{\max}=\tilde{\Phi}_1|_{A=1}\approx 1.12\sqrt{g/k}$. For (a)–(d) $N=2$ is the order of approximation, $n=1$, 2, 3; for $A\to 0\,|\Phi_{2,A}/\Phi_{1,A}|=|\tilde{\Phi}_{2,4}/\tilde{\Phi}_{1,A}|=2/5\approx e^{-0.92}$ and $|\Phi_{3,A}/\Phi_{1,A}|=|\tilde{\Phi}_{3,4}/\tilde{\Phi}_{1,A}|=1/15\approx e^{-2.71}$.

$$\omega_{3D\text{-}2D}=\sqrt{3}(k_y/k_x)\sqrt{gk_x}[1-3(1-A)^2/512], \qquad (23a)$$

in agreement with Ref. [32], while for fluids with similar densities $A\sim 0$,

$$\omega_{3D\text{-}2D}=2\sqrt{2}A^{1/6}(k_y/k_x)\sqrt{gk_x}. \qquad (23b)$$

Therefore the 2D-3D instability of nonlinear RT bubbles develop much slower for $A\sim 0$ than in the case of $A\sim 1$, Fig. 4. A slight curving of the interface with $(\zeta_{1y}k_x^2/\zeta_{1x}k_y^2)\ll 1$ also reduces the growth rate of the dimensional crossover. The explicit expressions for functions $F_{\zeta(k)}$, F_{2D}, $f_{x/y}$, f_A in Eqs. (19)–(22) are cumbersome and are not presented here.

We conclude that in three-dimensional RTI, the isotropic coherent structures are stable, and anisotropic structures are unstable. Three-dimensional RT bubbles tend to conserve a nearly isotropic shape in the plane normal to the direction of gravity. The nonlinear 2D bubbles are unstable under 3D modulations, and the dimensional 2D-3D crossover is discontinuous. Anisotropic 3D bubbles with other symmetry groups (*cmm* with two-parameter family of regular asymptotic solutions, and *p*2 with three-parameter family, Fig. 2) are unstable as well.

VI. DISCUSSION AND CONCLUSION

The foregoing results suggest the following dynamics of the bubble front in the Rayleigh-Taylor instability for fluids with a finite density ratio in the case of small initial perturbation. For isotropic highly symmetric 3D flows with spatial period λ in the plane normal to the direction of gravity (square *p*4*mm* or hexagons *p*6*mm*), the bubble curvature $\zeta(t)$, and velocity $\nu(t)$ grow as $\sim\exp(t/\tau)$ in the linear regime $t\ll\tau$, where $\tau\sim\sqrt{\lambda/Ag}$, and reach finite values $\zeta_1\approx\zeta_A$ and $\nu\approx\nu_A$ asymptotically for $t\gg\tau$. The parameters ζ_A and ν_A depend strongly on the Atwood number Eqs. (10), (15). For $A<1$ the bubbles are slower and less curved compared to the case of $A=1$, Eqs. (10), (15) [7]. The value of $\nu_A^2/g\lambda^4|\zeta_A|^3$ is the density ratio independent invariant of the flow, Eqs. (12), (17).

For anisotropic 3D flows with low symmetry and two spatial periods $\lambda_x<\lambda_y$ (rectangle *p*2*mm*), the bubble curva-

TABLE I. The values of the Fourier amplitudes $\Phi_{n,A}$, $\tilde{\Phi}_{n,A}$ with $n=1,2,3$ and velocity ν_A of the physically significant solutions for the 2D and highly symmetric 3D flows in the limiting cases of $A=1$ and $A\approx 0$ for $N=2$; in three dimensions the most isotropic symmetry $p6mm$ is chosen for a transparent comparison, the velocity $\nu_A=-\Sigma_n\Phi_{n,A}=\Sigma_n\tilde{\Phi}_{n,A}$.

	$A=1$, 3D	$A\approx 0$, 3D	$A=1$, 3D	$A\approx 0$, 2D
$\frac{\Phi_{1,A}}{\sqrt{g/k}}$	$-\frac{7}{6}$	$-\frac{5}{2}\sqrt{\frac{15}{17}}\sqrt{A}$	$-\frac{43}{36\sqrt{3}}$	$-\frac{5}{\sqrt{14}}\sqrt{A}$
$\frac{\Phi_{2,A}}{\sqrt{g/k}}$	$\frac{1}{6}$	$\sqrt{\frac{15}{17}}\sqrt{A}$	$\frac{7}{36\sqrt{3}}$	$\sqrt{\frac{2}{7}}\sqrt{A}$
$\frac{\Phi_{3,A}}{\sqrt{g/k}}$	$-\frac{1}{18}$	$-\frac{1}{2}\sqrt{\frac{5}{51}}\sqrt{A}$	$-\frac{7}{108\sqrt{3}}$	$-\frac{1}{3\sqrt{14}}\sqrt{A}$
$\frac{\tilde{\Phi}_{1,A}}{\sqrt{g/k}}$	$\frac{1577}{822}$	$\frac{5}{2}\sqrt{\frac{15}{17}}\sqrt{A}$	$\frac{13501}{6948\sqrt{3}}$	$\frac{5}{\sqrt{14}}\sqrt{A}$
$\frac{\tilde{\Phi}_{2,A}}{\sqrt{g/k}}$	$-\frac{893}{822}$	$-\sqrt{\frac{15}{17}}\sqrt{A}$	$-\frac{7705}{6948\sqrt{3}}$	$-\sqrt{\frac{2}{7}}\sqrt{A}$
$\frac{\tilde{\Phi}_{3,A}}{\sqrt{g/k}}$	$\frac{551}{2466}$	$\frac{1}{2}\sqrt{\frac{5}{51}}\sqrt{A}$	$\frac{4807}{20844\sqrt{3}}$	$\frac{1}{3\sqrt{14}}\sqrt{A}$
$\frac{\nu_A}{\sqrt{g/k}}$	$\frac{19}{18}$	$5\sqrt{\frac{5}{51}}\sqrt{A}$	$\frac{115}{108\sqrt{3}}$	$\frac{5}{3}\sqrt{\frac{2}{7}}\sqrt{A}$

tures change as $\zeta_{1x(y)}(t)\sim\exp(t/\tau_{x(y)})$ in the linear regime $t\ll\tau_x$, where $\tau_{x(y)}\sim\sqrt{\lambda_{x(y)}/Ag}$, and the growth of velocity $\nu(t)$ is dominated by the smaller period $\sim\exp(t/\tau_x)$. In the nonlinear regime $t\gg\tau_x$, the x components saturate faster than the y components, and secondary instabilities develop. The 3D bubbles in RTI tend to conserve an isotropic shape in the plane normal to the direction of gravity, and the dimensional 2D-3D crossover is discontinuous. In the nonlinear regime, the 2D-3D instability develops much slower for fluids with similar densities $A\sim 0$ compared to the case of fluids with highly contrasting densities $A\sim 1$, for a bubble with a shape curved in both directions compared to the case of a bubble curved in one direction and flattened in the other directions, and for smaller values of the aspect ratio λ_x/λ_y, Fig. 6, Eqs. (21)–(23).

To study the effect of the density ratio on the large-scale coherent dynamics in RTI, we separated scales in the governing equations (1), (2), identified all symmetry groups, which provide stability of the coherent structure under large-scale modulations [31], Figs. 1, and derived from the conservation laws a dynamical system (5) describing the evolution of the bubble front in a vicinity of its tip. Yet, the system (5) has the closure problem. To capture the interplay of harmonics one should account for the nonlocal properties of the flow that has singularities. We resolved this issue based on symmetry arguments. We considered all local solutions allowed by symmetry of the global flow, Fig. 2, found a continuous family of regular asymptotic solutions, and chosen the fastest stable solution in this family as the physically significant one, Eqs. (10), (15). The problem thus formulated does not require detailed information on nature and evolution of singularities. The results obtained indicate that the higher-order correlations influence significantly the values of the diagnostic parameters.

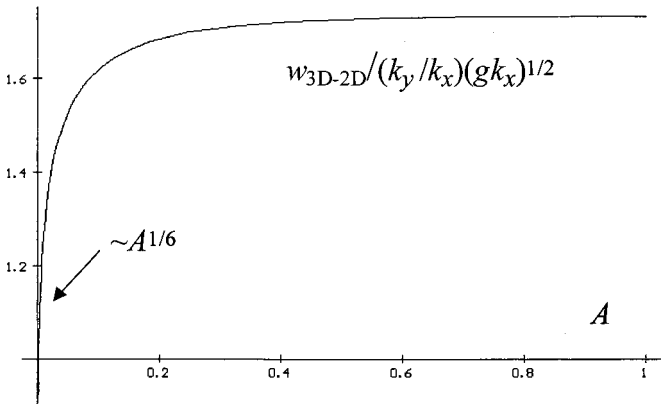

FIG. 6. The dimensional 2D-3D crossover for the RT bubbles; $k_{x(y)}$ is the wave vector in the $x(y)$ direction; g is gravity; the Liapunov exponent $\omega_{2D\text{-}3D}$ from Eq. (22) for nearly 2D bubbles with $\zeta_y=0$ and $\zeta_x=\zeta_A$ from Eqs. (15).

Empirical models [3,9] presumed the density-ratio independent invariant of the flow being the bubble curvature, with $|\zeta|\lambda=\pi/4$ in three dimensions and $|\zeta|\lambda=\pi/3$ in two dimensions, and employed the heuristic equation, which balanced with free parameters the flow inertia, buoyancy, and drag. The empirical model [3] adjusted the free parameters so that the bubble velocity given by Layzer's solution [20] for $A=1$ is re-scaled in the nonlinear regime as $g\to gA$ for $A<1$. The drag model [9] suggested re-scaling $g\to 2gA/(1+A)$. As discussed in Sec. IV, the assumptions of the heuristic models [3,9] can be derived via a single-mode approximation, only if one of the boundary conditions (2) is violated and the conservation laws are not obeyed. However, as over recent two decades many experiments and simulations were linked to the models [3,9], we compare here our multiple-harmonic solution with the single-mode solutions (ζ_L,ν_L) and (ζ_D,ν_D).

For the bubble velocity, the dependencies ν_D and ν_L are on one hand in reasonable agreement with experiments and simulations [3,6,12–17,34], and on the other hand violate the conservation laws (2). This controversy is apparent and can be easily explained. Figure 3 shows that in RTI for finite values of A, the bubble velocity is relatively insensitive to

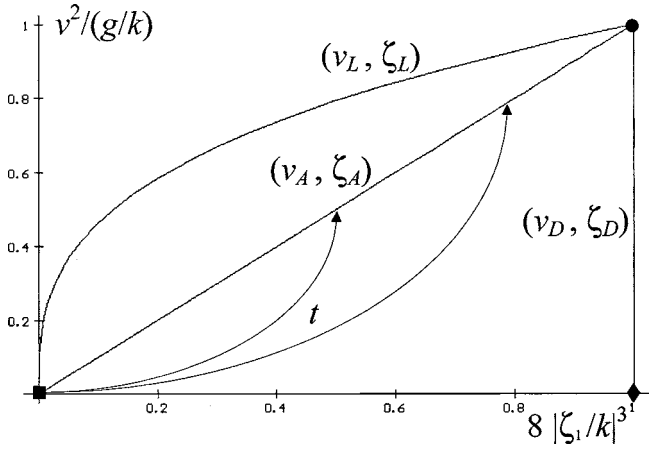

FIG. 7. The phase diagram; the bubble velocity $v(t)$ versus bubble curvature $\zeta_1(t)$ with time t being a parameter, $0 \leqslant A \leqslant 1$; The curves with arrows represent schematically the bubble front evolution from the linear, $(t/\tau) \sim 0$, to the nonlinear regime, $(t/\tau) \to \infty$, for two distinct Atwood numbers. The asymptotic values of the bubble velocity and curvature are given by the solutions (ν_A, ζ_A), (ν_L, ζ_L), and (ν_D, ζ_D). The black circle marks the solution $(\nu_{A(L,D)}, \zeta_{A(L,D)})$ with $A=1$, the black square marks the solution $(\nu_{A(L)}, \zeta_{A(L)})$ with $A=0$, the black diamond marks the solution (ν_D, ζ_D) with $A=0$.

detail of the interface dynamics, and the quantitative distinctions among the values of ν_A, ν_D, and ν_L is insignificant. Figure 4 shows the asymptotic values of bubble curvatures ζ_A, ζ_D, and ζ_L. For $A=1$ these values coincide, $\zeta_A=\zeta_L=\zeta_D$, [7,8], however, for $A \leqslant 0.6$ the quantitative difference among ζ_L, ζ_D, and ζ_A increases. In the limiting case of $A \to 0$, the ratio between the curvatures from Eq. (13b) and from the models [9,11] approaches $(\zeta_A/\zeta_D) \sim A^{1/3} \to 0$, while for the Layzer-type solution $(\zeta_A/\zeta_L) \sim A^{-2/3} \to \infty$, Eqs. (8a), (13b). We emphasize that for $A=0$ RTI does not develop and the bubble curvature should remain zero for all t, in agreement with our solution Eqs. (10), (13b).

We see that the bubble curvature is relevant and sensitive diagnostics parameter. This parameter determines the flow drag and can be used to address the following issue: Is the nonlinear evolution of RTI a single-scale or a multiscale process? If indeed this would be a single-scale process, as presumed by models [3,9,11], then the spatial period λ would define uniquely the shape of the bubble front as $\zeta \sim 1/\lambda$ and the drag force as $\sim \nu^2 |\zeta|^{-2} \sim \nu^2 \lambda^2$. Our theory identifies the density-ratio independent invariant of the large-scale coherent dynamics as $\nu_A^2/g\lambda^4|\zeta_A|^3 = (dh/dt)^2/g\lambda^4|\zeta_A|^3$. This invariant indicates that the bubble front is parabolic, and its shape depends on the two length scales as $\zeta_A \sim [(dh/dt)^2/g\lambda^4]^{1/3} \sim \mathrm{Fr}^{1/3}/\lambda$. Therefore the horizontal scale λ and the vertical scale h contribute independently to the flow drag and to the nonlinear dynamics, Fig. 1(a). The evolution of the large-scale coherent structure in RTI is a multiscale process.

The results obtained are summarized in the phase diagram in Fig. 7, which represents schematically the bubble velocity $v(t)$ versus bubble curvature $\zeta_1(t)$ with time t being a parameter and for the values of the Atwood number from the interval $0 \leqslant A \leqslant 1$. Initially for $(t/\tau)=0$ the perturbation is small, and for any density ratio the phase trajectory starts near the point $(0,0)$ in the units of $8|\zeta/k|^3$ and $v^2/(g/k)$. Asymptotically $(t/\tau) \to \infty$ the bubble velocity and curvature approach finite values dependent on the Atwood number. The asymptotic values of the bubble velocity and curvature for solutions (ν_A, ζ_A) are presented in Fig. 7 by the straight line with $\nu_A \sim 0$, $\zeta_A \sim 0$ for $A \sim 0$ and $\nu_A \sim \sqrt{g/k}$, $\zeta_A \sim -k/8$ for $A \sim 1$. The drag model solutions with $\nu_D = \sqrt{2Ag/(1+A)k}$ and $\zeta_D = -k/8$ are presented in Fig. 4 by the vertical line, while the Layzer-type solutions with $\nu_L = \sqrt{Ag/k}$ and $\zeta_L = -Ak/8$ are given by the curved line. According to our theory, the phase trajectory should hit the straight line (ν_A, ζ_A) asymptotically, as $(t/\tau) \to \infty$, at a point determined by the value of the Atwood number, as shown in Fig. 7, neither the vertical line given by (ν_D, ζ_D) nor the curve given by (ν_L, ζ_L).

The lack of data prevents us from a detailed quantitative comparison with observations. For most existing experiments and simulations, the measurement of the bubble curvature requires an improvement of diagnostics. Our results show that the bubble curvature is important diagnostic parameter, whose value indicates whether the normal component of velocity is continuous at the interface, whether there is a mass flow across the interface, and whether the mass flow is conserved.

Experiments and simulations [17,35,36] have shown that in RTI three dimensional bubbles form a close packing in the plane normal to the direction of gravity and have a nearly isotropic shape, while 2D flows become eventually three dimensional. Our results agree with these observations qualitatively. On the other hand, experiments [15] reported that for fluids with similar densities the RT bubbles remains nearly two dimensional in the nonlinear regime of the instability. Our theory explains the experiments [15] as well. For small values of the Atwood number the 2D-3D instability develops slowly [Eq. (16)], and experiments [15] may not have enough time to observe it. Owing to the lack of observation data, we cannot perform a detailed quantitative comparison here. There is a need for systematic experimental and numerical study of secondary instabilities in anisotropic RT flows and their dependencies on the density ratio and the initial conditions.

Spectrum is another important diagnostics of the flow. Our multiple harmonic analysis suggest that, as long as the flow dynamics is governed by a dominant mode, the values of the Fourier amplitudes decay with increase in their number, and the Fourier amplitudes for the light fluid are larger than those for the heavy fluid (Fig. 3 and Table I). However, the spectral properties of the nonlinear dynamics in RTI are rarely monitored, [17], and we cannot compare our results with observations. Finally, our results show that in contrast to suggestions of Ref. [11], the dynamics of the RT spike cannot be described via the approach of the Layzer type. To depict the spike motion, one may look for a similarity solution for Eqs. (2). Reference [37] recently reported a similarity solution describing the spike dynamics in the system fluid-vacuum with $A=1$. For a two-fluid system with $A<1$, the problem is much more complicated and we address it in the future.

In conclusion, our theory describes the principal influence of the density ratio on the dynamics of the nonlinear bubbles in the Rayleigh-Taylor instability. Our results indicate a nonlocal and multiscale character of the large-scale coherent dynamics. The foregoing analysis is based on the assumptions that the period of the coherent structure is invariable, the transfers of energy to smaller or larger scales are not extensive, and the vorticity does not change the time dependence of the coherent motion. For fluids with very similar densities $A \approx 0$ and for a large amplitude initial perturbation, these requirements may be violated and our theory may be inapplicable. This paper does not study the multibubbles interactions and the merger mechanism of the turbulent mixing.

ACKNOWLEDGMENTS

This work was partially supported by the Naval Research Laboratory, DOE/ASC, and the Japanese Society for the Promotion of Sciences.

[1] Lord Rayleigh, *Scientific Papers, II* (Cambridge University Press, Cambridge, England, 1990); R. M. Davies and G. I. Taylor, Proc. R. Soc. London, Ser. A **200**, 375 (1950).
[2] R. D. Richtmyer, Commun. Pure Appl. Math. **13**, 297 (1960); E. E. Meshkov, Fluid Dyn. **4**, 101 (1969).
[3] D. H. Sharp, Physica D **12**, 3 (1984).
[4] F. Kull, Phys. Rep. **206**, 197 (1991).
[5] D. D. Ryutov *et al.*, Rev. Mod. Phys. **72**, 167 (2000); H. Takabe, Prog. Theor. Phys. Suppl. **143**, 202 (2001); W. Hillebrandt and J. C. Niemeyer, Annu. Rev. Astron. Astrophys. **38**, 191 (2000); V. V. Bychkov and M. A. Liberman, Phys. Rep. **325**, 116 (2000).
[6] M. Schneider, G. Dimonte, and B. Remington, Phys. Rev. Lett. **80**, 3507 (1998).
[7] S. I. Abarzhi, Phys. Rev. Lett. **81**, 337 (1998); Phys. Rev. E **59**, 1729 (1999).
[8] S. I. Abarzhi, K. Nishihara, and J. Glimm, Phys. Lett. A **317**, 470 (2003).
[9] U. Alon, J. Hecht, D. Offer, and D. Shvarts, Phys. Rev. Lett. **74**, 534 (1995); D. Oron, U. Alon, D. Offer, and D. Shvarts, Phys. Plasmas **8**, 2883 (2001).
[10] G. Dimonte, Phys. Plasmas **7**, 2255 (2000).
[11] V. N. Goncharov, Phys. Rev. Lett. **88**, 4502 (2002).
[12] K. Read, Physica D **12**, 45 (1984).
[13] Yu. A. Kucherenko *et al.*, Izv. Akad. Nauk SSSR, Mekh. Zhidk. Gaza **6**, 157 (1978); S. G. Zaytsev *et al.*, Sov. Phys. Dokl. **35**, 159 (1990).
[14] X. Y. He, R. Y. Zhang, S. Y. Chen, and G. D. Doolen, Phys. Fluids **11**, 1143 (1999).
[15] J. T. Waddell, J. W. Jacobs, and C. E. Niederhaus, Phys. Fluids **13**, 1263 (2001).
[16] G. Gardner *et al.*, Phys. Fluids **31**, 447 (1988); D. L. Youngs, Phys. Fluids A **3**, 1312 (1991).
[17] S. B. Dalziel, P. F. Linden, and D. L. Youngs, J. Fluid Mech. **399**, 1 (1999).
[18] S. Chandrasekhar, *Hydrodynamic and Hydro-magnetic Stability*, 3rd ed. (Dover Publications Inc., New York, 1981), pp. 428–477.
[19] D. L. Youngs, Physica D **12**, 32 (1984); Y. P. Chen *et al.*, Phys. Fluids A **5**, 29292 (1993).
[20] D. Layzer, Astrophys. J. **122**, 1 (1955).
[21] P. R. Garabedian, Proc. R. Soc. London, Ser. A **241**, 423 (1957).
[22] G. Birkhoff and D. Carter, J. Math. Mech. **6**, 769 (1957); Vanden Broeck, Phys. Fluids **27**, 1090 (1984); J. A. Zuffiria, *ibid.* **31**, 3199 (1988); G. Hazak, Phys. Rev. Lett. **76**, 4167 (1996).
[23] S. Tanveer, Proc. R. Soc. London, Ser. A **441**, 501 (1993).
[24] D. W. Moore, Proc. R. Soc. London, Ser. A **365**, 105 (1979).
[25] S. J. Cowley, G. R. Baker, and S. Tanveer, J. Fluid Mech. **378**, 233 (1999).
[26] D. I. Meiron, G. R. Baker, and S. A. Orszag, J. Fluid Mech. **114**, 238 (1982).
[27] M. Shelley, J. Fluid Mech. **119**, 507 (1992); T. Y. Hou, J. S. Lowengrub, and M. J. Shelley, Phys. Fluids **9**, 1933 (1997).
[28] K. Nishihara, Phys. Plasmas **3**, 376 (1996); C. Matsuoka, K. Nishihara, and Y. Fukuda, Phys. Rev. E **67**, 082303 (2003).
[29] H. Aref and G. Tryggvason, Phys. Rev. Lett. **62**, 749 (1989).
[30] L. D. Landau and E. M. Lifshitz, *Course of Theoretical Physics VI, Fluid Mechanics* (Pergamon Press, New York, 1987).
[31] A. V. Shubnikov and V. A. Koptsik, *Symmetry in Science and Art* (Plenum Press, New York, London, 1979). Basic elements for the group *p*6*mm* are periodicity in the (x,y) plane, sixfold axis of rotation and mirror planes of reflection normal to each other and parallel to the z axis. Groups *p*4*mm* and *p*2*mm* have a fourfold and twofold axis of rotation. Symmorphic groups have no glide planes and screw axes.
[32] S. I. Abarzhi, Phys. Fluids **13**, 2182 (2001).
[33] The Layzer-type single-mode solution (8a) does conserve momentum. With mass flux across the interface the terms $\rho_{h(l)} \times (\boldsymbol{v}_{h(l)} \cdot \boldsymbol{n})^2$ should be added in the momentum boundary condition (2b). In the expansion (5b), these terms are $\sim x^{2i} y^{2j}$, $i + j \geqslant 2$, and do not contribute to Eqs. (5b), (7b). With and without mass flux across the interface, the Layzer-type solution has in the linear regime the growth rate $\sim \exp(t\sqrt{gk})$, which coincides with the growth rate of the Landau-Darrieus instability in a gravity field in the limiting case of very large g; see Ya. B. Zel'dovich *et al.*, *The Mathematical Theory of Combustion and Explosions* (Consultants Bureau, New York, 1985).
[34] S. I. Abarzhi, J. Glimm, and A. Lin, Phys. Fluids **15**, 2190 (2003).
[35] M. M. Marinak *et al.*, Phys. Rev. Lett. **80**, 4426 (1998).
[36] M. F. Ivanov, A. M. Oparin, V. G. Sultanov, and V. E. Fortov, Dokl. Phys. **44**, 491 (1999).
[37] P. Clavin and F. A. Williams, J. Fluid Mech. **525**, 105 (2005).